JOURNAL OF RAMAN SPECTROSCOPY
J. Raman Spectrosc. 2005; **36**: 541–550
Published online in Wiley InterScience (www.interscience.wiley.com). DOI: 10.1002/jrs.1332

Tip-enhanced Raman spectroscopy (TERS) of malachite green isothiocyanate at Au(111): bleaching behavior under the influence of high electromagnetic fields

Bruno Pettinger,* Bin Ren,† Gennaro Picardi,‡ Rolf Schuster§ and Gerhard Ertl

Fritz-Haber-Institut der Max-Planck-Gesellschaft, Faradayweg 4–6, D-14195 Berlin, Germany

Received 19 November 2004; Accepted 1 February 2005

Tip-enhanced Raman spectroscopy (TERS) was investigated with malachite green isothiocyanate adsorbed at an Au(111) surface. TERS is based on the excitation of localized surface plasmons in the tip apex, producing strongly enhanced electromagnetic fields. The key conditions for giant TERS are side-illumination of the tip, well-prepared single-crystalline surfaces and sharp, smooth gold tips. A TERS enhancement of about 6×10^6 has been observed for dye molecules adsorbed at the Au(111) substrate in a region of about 50 nm diameter beneath the tip. This corresponds to a 2500-fold increase in the light intensity at the Au(111)/air interface, which in addition causes fast but local bleaching of the dye. This bleaching behavior was analyzed in detail, giving direct insight into the strength and size of the enhanced field. In addition, the bleaching constant was higher for MGITC in an unperturbed environment than for MGITC in an environment that had been substantially bleached. The MGITC spectra were also different for these two cases. Copyright © 2005 John Wiley & Sons, Ltd.

KEYWORDS: apertureless scanning near-field optical microscopy; gold(111); tip-enhanced Raman spectroscopy; malachite green isothiocyanate; near-field enhancement

INTRODUCTION

The general use of Raman spectroscopy for surface studies is an old dream of surface scientists. However, with differential Raman cross-sections of the order of $(d\sigma/d\Omega) \approx 10^{-31}$–$10^{-28}$ cm^2 sr^{-1}, surface studies were out of reach in general, although a (small) number of attempts were made to apply (normal) Raman scattering for the investigation of well-defined surfaces.

*Correspondence to: Bruno Pettinger, Fritz-Haber-Institut der Max-Planck-Gesellschaft, Faradayweg 4–6, D-14195 Berlin, Germany. E-mail: pettinger@fhi-berlin.mpg.de
†Present address: State Key Laboratory for Physical Chemistry of Solid Surfaces and Department of Chemistry, College of Chemistry and Chemical Engineering, Xiamen University, Xiamen 361005, China.
‡Present address: Biophysics and Nanoscience Centre, INFM Dipartimento di Scienze Ambientali Università della Tuscia, I-01100 Viterbo, Italy.
§Present address: Institute of Inorganic and Physical Chemistry, Technical University of Darmstadt, D-64287 Darmstadt, Germany.
Contract/grant sponsor: Alexander von Humboldt Foundation.
Contract/grant sponsor: National Science Foundation of China; Contract/grant number: 90206039; 20473047.
Contract/grant sponsor: 973 Project; Contract/grant number: 2001CB610506.
Contract/grant sponsor: Max Planck Society.

Recently, a new approach has been developed, denoted tip-enhanced Raman spectroscopy (TERS), in some cases also called 'apertureless scanning near-field optical microscopy (SNOM)'.[1] With the advent of TERS, the above-mentioned dream is now becoming a reality.[1–12]

TERS is a particular promising variant of SERS, the well-studied field of surface-enhanced Raman scattering spectroscopy. The latter requires roughened surfaces at which two cooperative enhancement mechanisms for Raman scattering are working. Roughened surfaces can support the excitation of localized surface plasmons leading to the so-called 'electromagnetic enhancement' and provide the peculiar adsorption sites at which the so-called 'chemical enhancement' is operative. In the literature, a large range of (total) enhancement factors are given, starting with the 10^6-fold enhancement found for pyridine on roughened silver electrodes[13] up to the giant 10^{12}–10^{14}-fold enhancement reported more recently by Nie and Emory[14] and Kneipp *et al.*[15] for dyes at colloidal particles. In the latter case, the authors claim to have reached single-molecule detection sensitivity. However, in all these cases the general drawback of SERS investigations remains: the surface enhancement (in particular its 'chemical' part) and the molecule–substrate interaction, both occurring at unspecified sites, are nearly

inseparably interconnected. This renders the analysis of spectroscopic data difficult. In contrast to the (comparatively easy) case of interfacial infrared spectroscopy, in SERS questions such as on the molecular orientation and binding sites of adsorbates can hardly be answered. Nevertheless, SERS has been used successfully in numerous studies.

Recently, it has been observed that only a very small fraction of adsorbed molecules contribute to SERS. The concept of *hot spots* was born: a rough surface can be considered as a fractal, with some self-similarity between large- and small-scale structures.[16,17] If there is field confinement for the former, a correspondingly stronger field confinement must exist for the latter, which means the smaller are the structures, the higher is the enhancement of the electromagnetic field. Because the Raman enhancement scales with the fourth power of the field enhancement, a few small structures can create more SERS than the rest of the rough surface. Ultimately, a single, very small structure and its adsorbate, such as a particle dimer and a single or a few adsorbed molecules, may produce Raman scattering which is sufficiently intense to be recorded. This concept may explain also the single-molecule sensitivity of SERS reported by Nie and Emory,[14] Kneipp *et al*.[15] and Meixner *et al*.[18]

In a sense, TERS is a variant of the idea of hot spots (although it has been developed along a somewhat different route). The main idea is to use the illuminated apex of an AFM or STM tip made of a suitable material as a near-field enhancer. That means that the enhanced field is present only in the close vicinity of the tip apex. If the tip is kept at a small distance above an adsorbate-covered substrate, only adsorbates underneath the tip participate in TERS. In this way, the interaction of adsorbates with a substrate and the enhancement provided by the tip are completely decoupled, in contrast to the case of SERS. Moreover, because of the local nature of the enhanced field, TERS promises to permit Raman microscopy with sub-wavelength resolution down to the nanometer region.

TERS has been developed out of the field of scanning near-field optical microscopy (SNOM or NSOM), which combines a scanning probe device with an optical near-field instrument such as a tapered fiber tip. Of particular interest and advantages were the cases where the emitted/recorded photons have different energies to the incident radiation such as fluorescence[19] or Raman scattering processes.[20–22] Soon it turned out that this near-field concept has conflicting requirements: for a high throughput (to achieve intense signals), the aperture of the fiber tip should be large, whereas for a high spatial resolution, the aperture should be as small as possible. Unfortunately however, fundamental considerations show that the spatial resolution of SNOM can hardly be better than 30–50 nm.[23,24] To overcome the limitation of low transmission of fiber tips, the so-called apertureless near-field optical microscope (A-SNOM) was developed.[23,24] In this approach, either a metal particle is attached to the tip apex or the tip is coated with a thin metal film, or the tip is made from a metal wire, for example by etching techniques. In most cases, the metal used is either silver or gold. If such a tip is illuminated, localized surface plasmons are excited at the tip apex or at the tip–substrate cavity. This results in large enhancements of the electromagnetic field in the vicinity of the tip apex relative to the incident one. Hence these enhanced fields locally drive optical processes such as fluorescence and Raman scattering at an increased rate. This approach, now applied to inelastic light scattering, became known as tip-enhanced Raman spectroscopy (TERS).

Theoretical studies on TERS report field enhancements g up to three orders of magnitude in particular wavenumber regions (see, for example, Refs 25–31). Hence, owing to the fourth-power rule, $F_{\text{enhanced Raman}} = g^4$, there should be a TERS enhancement by up to 12 orders of magnitude. Such a prediction, however, contrasts drastically (so far) with experimentally observed enhancement factors, which are from around three to nearly seven orders of magnitude.[1–12] (In that context, it should be mentioned that even for SERS there are a few experimental and theoretical studies reporting extremely high enhancement factors, i.e. $F_{\text{SERS}} > 10^8$.[14,15] Note, for example, the concept of Shalaev and co-workers of a few 'hot spots' being responsible for most of the SERS signal.[16,17] From this point of view, *the potential of TERS for similar giant enhancements seems not to have been met yet*.)

The first approach to apertureless near-field Raman spectroscopy was designed by the Zenobi group. Stöckle *et al*.[1] reported a significant enhancement of the Raman signal if a metalized AFM tip is brought within a few nanometers of a dye film deposited on a glass substrate. They reported a more than 30-fold net increase in the Raman signal by the tip. (By the 'net increase' we mean the n-fold increase of the overall Raman signal in the presence of the tip compared with the Raman intensity in the absence of the tip.) Taking into account the small area of the enhanced field underneath the tip of <50 nm diameter, a 2000-fold enhancement of Raman scattering in the vicinity of the tip has been deduced. Similar effects were reported for C_{60} molecules and an electrochemically etched Au tip with an apex 20 nm in diameter (this tip is mounted in a shear-force set-up).[1] In addition, the authors also noted that this approach has a spatial resolution of about 55 nm.

Only a few months later, Anderson[2] described a very similar experiment, using an AFM tip covered with layer of gold grains with a average size of 45 nm to enhance the Raman scattering from a sulfur layer on a quartz substrate. If the tip was moved 15 μm away from the substrate, no Raman signal of sulfur was detectable, but with the tip operated in contact mode a spectrum with high signal-to-noise ratio could be observed. An enhancement factor of >10 000 was estimated.[2]

Also in 2000, Hayazawa *et al*.[3] subsequently reported the next study on apertureless SNOM using a silver-coated cantilever and a dye-coated silver film on a glass slide.

The dye was rhodamine 6G. A 40-fold enhancement of Raman scattering was observed with 488 nm excitation; an enhancement of fluorescence was also seen.[3] The authors observed bleaching behavior for rhodamine 6G, but they did not mention whether or not the bleaching rate was tip enhanced. Instead, they pretreated this system by 20 min illumination until a stationary state had been reached.

At the end of 2000, Pettinger *et al*.[10] presented a TERS study using for the first time an STM device. The system investigated was brilliant cresyl blue (BCB) adsorbed on a smooth thin gold film (12 nm) evaporated on a glass slide, and the tip was an etched silver wire. The overall set-up was similar to that of Stöckle *et al*.[1] The adsorption procedure resulted in (sub)monolayer coverage of the dye. Under these conditions, the dye fluorescence was effectively quenched by the metal film and a weak resonance Raman signal was detectable in the absence of the STM tip. If the tip was brought into the tunneling position (~1 nm above the surface), a 16-fold net increase could be observed.[11] Since in these experiments the tip radius was large (100–500 nm), only a comparatively weak average enhancement was noted. The authors addressed the point that the enhancement must have a sharp radial profile. In the highest field zone at the center of the tip apex it may reach values between 10^3 and 10^4.[10]

Characteristic for many of the above-described experiments and other TERS studies reported in the literature are the use of (i) an inverted microscope or a kind of illumination that is closely related, (ii) thick sample films and (iii) tips covered with metal grains. Each of these points bear problems in the sense of non-optimal TERS conditions. In fact, a configuration optimal for TERS requires (i) illumination with a strong polarization component parallel to the tip axis, (ii) the possibility of using opaque, massive substrates, (iii) easy control of the adsorbate coverage on the substrate and (iv) sharp and smooth tips with narrow apexes and narrow cones. The production of suitably shaped tips is a crucial part of any TERS experiment.[32–34]

Our recent TERS approach combines *side illumination with sharp tips* and allows for the investigation of *single crystalline substrates*. This configuration yielded giant enhancements for small and large molecules and for optically non-resonant and optically resonant molecules; TERS was observed for crystalline gold and platinum substrates.[32,34] Therefore, we consider this approach to be a significant step towards the more general application of TERS in surface studies. In this context it should be noted that for most experiments up to now net gains in Raman scattering between 1.5 and 40 were reported; with our set-up we recently observed net gains up to 8000, pointing towards a local TERS enhancement of $>10^6$, in addition to fast bleaching of the molecules in the presence of the tip.[32]

In the present paper, we focus on a detailed analysis of the bleaching effect. In contrast to an earlier approach based on the assumption of a constant field profile,[32] we will use a radially varying profile of the enhanced field for the analysis of the experimental data. The aim is to model the decay of the TERS intensities during the bleaching, to identify the nature of the adsorbed species and to gain further insight into the distribution of the enhanced electromagnetic field underneath the tip. In addition, the dependence of TERS on the tip–substrate distance is modeled and compared with experimental results in the literature.

We chose MGITC adsorbed on a smooth Au(III) single-crystalline surface as a test system and an Au tip for the local field enhancement. The theory predicts that a tip-metal configuration, such as Au tip/gold substrate configuration, is particularly suitable for optimal excitation of localized surface plasmons. To avoid complications associated with SERS in addition to TERS, very smooth surfaces are needed, which do not support SERS. Hence well-annealed single-crystalline metal surfaces were used as substrates. MGITC was employed as a dye because of its large resonant Raman scattering (RRS) cross-section at the illumination wavelength.

EXPERIMENTAL

The sample was illuminated with radiation from an He–Ne laser ($\lambda_{ex} = 632.8$ nm), which was passed through a 50× long working distance objective of an Olympus microscope and directed on to the sample surface at an angle of incidence of 60°. The scattered light was collected in backscattering geometry through the same objective and transferred through a notch filter into the Raman spectrograph (LabRam 1000). Both the positions of the substrate surface and the STM tip could be adjusted with respect to the laser focus by *x*,*y*-translation stages. The movement of the STM tip towards the surface was performed first by a coarse mechanical approach and then by a piezo tube controlled by electronic feedback. The focusing of the light and the coarse approach of the tip to the sample were monitored and controlled with an auxiliary microscope and a CCD camera.

The experiments were performed with smooth single-crystalline Au(111) surfaces, which had been prepared by flame annealing to obtain a well-defined surface structure and to remove possible contaminants.[35] For the formation of a submonolayer of dye molecules, the crystal was wetted with a droplet of a 10^{-6} M ethanolic MGITC dye solution, which dried off quickly. The total amount of dye present was significantly below a monolayer with respect to the substrate atoms. During the drying of the droplet, the dye was adsorbed irreversibly at the metal through its sulfur atom and formed, in particular in the inner region of droplet and, hence, in the inner region of the probed sample surface, a self-assembled (sub-)monolayer. Subsequently, the crystal was washed with copious amounts of ethanol, to remove all dyes not directly bound to the metal (i.e. all dyes were removed, which were adsorbed in possible second and further layers). The STM tip was in most cases prepared from a gold wire of 0.25 mm diameter by electrochemical etching

in a 1 : 1 mixture of ethanol and fuming HCl, yielding typical tip radii of about 30–60 nm.[33,34] STM images were recorded with either Au or Ir tips and showed that the surfaces studied were fairly smooth, exhibiting essentially only monoatomic steps.

For TERS experiments, the STM tip was positioned on a large single-crystalline Au(111) terrace. The tip and laser focus were aligned using strongly reduced white light and He–Ne laser intensities. Subsequently, the tip was retracted and first an RRS spectrum was recorded (i.e. the tip was in the retracted position). Subsequently, the laser light was switched off, the STM tip was placed in the tunneling position, the laser light was switched on and a series of Raman spectra were recorded with a 1 s acquisition time and about a 1 s delay. Since our present configuration is operated in air and not under UHV conditions, detailed information about the chemical state of the sample surfaces is not available.

If the STM tip is brought into the tunneling position at about 1 nm distance above the surface (carefully avoiding accidental contact), an optical cavity is formed. Such a cavity has particular optical modes, which are called localized surface plasmons (LSPs) and which can be excited by placing this cavity in the focus of the laser light. The LSPs are associated with electron density oscillations in the tip and the surface under the influence of the external electromagnetic field, creating in turn their own local electromagnetic field. Only a small part of the molecules, which are located in the close vicinity of the tip apex and which are therefore exposed to this enhanced field, contribute to TERS.

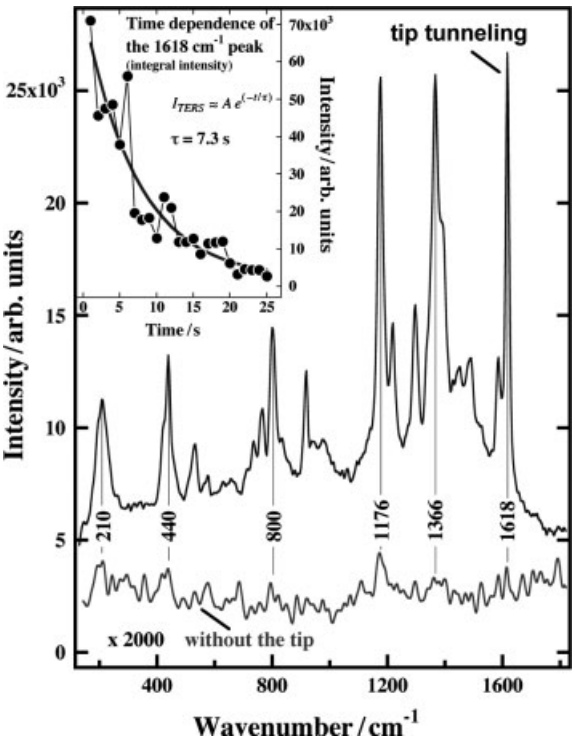

Figure 1. Comparison of RRS and TERS spectra for MGITC adsorbed on an Au(111) surface. The laser power in the TERS case is reduced to 0.5 mW; the spectral intensities are normalized to full laser power (5 mW) and acquisition time 1 s. The actual acquisition times were TERS 1 s and RRS 60 s. The MGITC dye is adsorbed from a 10^{-7} M ethanol solution for 30 min. Tunneling current, 1 nA; voltage, −150 mV. Inset: time dependence of the integral intensity of the 1618 cm^{-1} band for reduced laser power. (Reprinted with permission from Ref. 32).

RESULTS

TERS and bleaching for MGITC at gold(111) surfaces

Figure 1 shows the Raman spectra of MGTIC on Au(111) in the absence and presence of the tunnelling Au tip.[32] The TERS signal was on average about 8000 times larger than the RRS signal of the dye in the absence of the tip (see Fig. 1). The bleaching behavior of the peak at 1618 cm^{-1} is depicted in the inset in Fig. 1. These data were recorded at a 10-fold reduced laser intensity. The measured time constant of 7.3 s therefore corresponds to a bleaching time constant of 0.73 s at full laser power, which has to be compared with the bleaching time constant of 800 s for the resonance Raman scattering (RRS) of the adsorbed dye in the absence of the tip. This difference has been related to the gain in the electromagnetic field strength underneath the tip apex and permitted the estimation of the field enhancement to $g_{TERS} \approx 33$. Consequently, owing to the g^4 law for the TERS enhancement, a $>10^6$-*fold* average TERS enhancement has been determined, with a radius of the enhanced field of ~90 nm.[32] We noticed that for such a giant enhancement particular tips are required, presumably tips that have a smooth surface and a sharp apex (radius <50 nm). Therefore, substantial effort has been devoted to elaborating procedures for the easy production of suitable tips, based on electrochemical etching techniques as described in a paper by Ren *et al*.[33] We are now able routinely to fabricate tips with an apex radius of $R_{tip} \leq 30$ nm.

At first glance, bleaching processes seem to hamper TER spectroscopy. However, within the observed time dependencies and within the variation of the spectroscopic features interesting and important information is encoded. Hence it is desirable and necessary to investigate the bleaching processes in more detail, both experimentally and theoretically.

The experimentally observed bleaching behavior is represented by a three-dimensional plot of the TERS intensity versus Raman shift and total time in Fig. 2. Note that a reduced laser power was used (0.5 mW). An initial time constant of about 6 s can easily be estimated from the rapid decrease in intensity at the beginning. It is also evident that different bands are differently affected by the bleaching. These effects will be discussed in more detail below. Additionally, there are remarkable general intensity fluctuations, for example, the dip in the time interval between

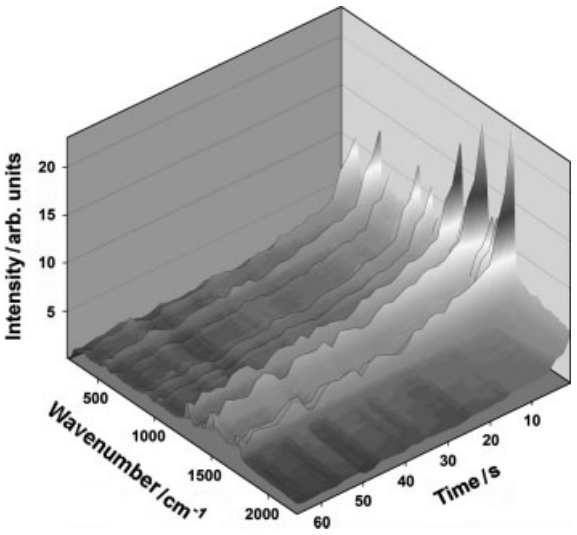

Figure 2. Three-dimensional plot of the TERS intensity vs wavenumber and time. This plot is made from the different series of spectra in Fig. 1. Laser power, 0.5 mW; acquisition time, 1 s; delay, 1 s.

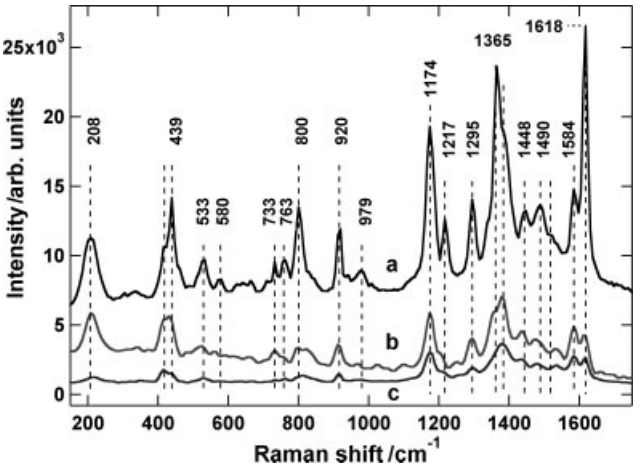

Figure 3. Spectra of MGITC adsorbed on an Au(111) surface. (a) 'Unbleached' TERS spectrum of MGITC; (b) TERS spectrum from species embedded in a partly bleached environment; (c) averaged spectra of the last five spectra of a series of 39 spectra recorded with a total interval of 2 s. Acquisition time, 1 s.

45 and 50 s for all wavenumbers. Fluctuations of this type affect all Raman bands and are far too large to be explained by noise, which is relatively low due owing the large TERS intensities.

Most of the bleaching and the associated changes in intensities and spectral characteristics occur within the first few seconds. Even the first recorded spectrum inevitably contains characteristics of these effects. Hence it is desirable to reconstruct from the measured spectra the spectrum of the unbleached MGITC layer and also the spectrum from (partly) bleached MGITC. Assuming a linear superposition of spectra of unbleached and bleached MGITC, we deconvoluted the data in Fig. 2 shortly after beginning illumination, employing the algorithm presented in the Appendix. Figure 3 presents the results. Curve a represents the (hypothetically) unbleached spectrum of MGITC and spectrum b is the spectrum for MGITC in a (partly) bleached environment. These are compared with a spectrum c containing the averaged sum of the last five spectra of Fig. 2, showing the result of extended bleaching. The vertical dashed lines indicate that all three spectra exhibit essentially the same spectral bands, but with different absolute and relative intensities and in some cases with different bandwidths. We attribute these changes to the growing disorder in the self-assembled (sub-)monolayer of the dye, caused by the bleaching processes. For example, photofragmentation of the dye leads to changes in the surrounding of unfragmented dye molecules and therefore alters the distinct coupling of individual molecules with its environment. However, we emphazise that all three spectra a, b and c are spectra of MGITC, because most bands are only modified in their relative intensities and

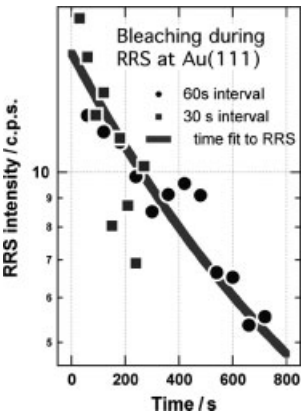

Figure 4. Time dependence of the RRS signal of MGITC adsorbed on an Au(111) surface. Filled squares and circles represent experimental data; the solid line is a fit curve for a time constant of 660 s.

not in their wavenumbers. Only a few bands are slightly shifted in wavenumber. Let us now discuss only the most spectacular change, i.e. the rapid vanishing of the 1618 cm^{-1} vibration. Within 70 s of illumination its intensity drops to one-twentieth of its initial value, while the neighboring band at 1584 cm^{-1} drops 'only' by one-quarter. Apparently, the band at 1618 cm^{-1} is much more sensitive to disorder and photofragmentation than that at 1584 cm^{-1}, and the ratio of these two peak intensities can be seen as reflecting the progress of the disorder/bleaching present in the layer. It is noteworthy that during the alignment procedure of the tip and laser focus, part of the dye layer was exposed to weak light intensities. Hence even in spectrum a some bleaching had already occurred.

Figure 4 shows the resonance Raman intensity of the 1618 cm^{-1} band of adsorbed MGITC versus time (squares and circles) in the absence of the tip in a semi-logarithmic plot. The experimental data were recorded with 30 and 60 s acquisition time, respectively, and negligible delay. As is apparent from the semi-logarithmic plot, the bleaching data cannot be described by a first-order rate law, i.e. by an exponential decrease in intensity with time. This can be explained considering the spatially strongly varying intensity profile in the focal area of the illuminating laser, which causes radially varying bleaching rates. The fit to the data (solid line) was calculated using Eqn (A11), which takes a Gaussian intensity profile in the laser spot into consideration, and which will be discussed in detail below. The fit resulted in an initial bleaching time constant of 660 s.

For comparison, Fig. 5 shows again the TERS intensity of the 1618 cm^{-1} band versus time, taken from the series of spectra in Fig. 2 on a semi-logarithmic scale. Similarly to the bleaching behavior in the absence of the tip (Fig. 4), a simple exponential rate law is not sufficient to explain completely the observed behavior. Considering a radially varying intensity distribution of the enhanced field around the tip apex can almost perfectly account for the experimental data; however, only if one takes two different bleaching processes into account, each of them deviating from the simple exponential rate law. The solid line presents a corresponding fit to the data assuming again a Gaussian intensity distribution of the enhanced field. It is calculated according to Eqn (A12), discussed below. The initial time constant is about 6 s; normalized to the full laser power, the time constant is 0.6 s.

Let us consider the fits. First the RRS case is treated, resulting in the fixing of a few parameters such as the numerical product of bleaching constant and intensity. These parameters must be used also for the fit of the TERS curve. Free parameters are then only the field enhancement g and the size of the enhanced field R_{field}. It turned out that the experimental TERS data could not be fitted with a single fit curve. Instead, two fit curves (each of them deviating from a first-order rate law as a consequence of the radially varying field profile) were necessary for the TERS case, with distinctly different bleaching constants and amplitudes, but with the same values for g and R_{field}. Obviously, the experimental results show not only spectral changes for MGITC in different environments (see Fig. 3), but also a significantly different bleaching behavior for MGITC in an intact environment and MGITC in a disordered/bleached environment. A possible explanation might be a less vertical orientation of MGITC in a bleached surrounding compared with a more vertical orientation for MGITC with non-bleached neighbor molecules. This affects both the TERS intensity and the bleaching rate: the more compact and intact MGITC layer shows a higher TERS intensity and a faster decay than MGITC in a bleached environment (if one extrapolated both fit curves to $t = 0$).

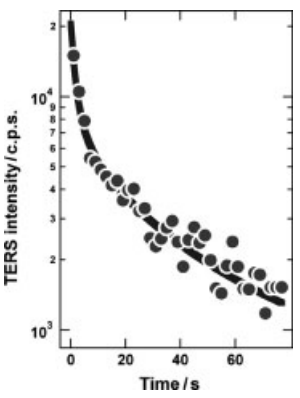

Figure 5. Time dependence of the TERS intensity of the 1618 cm^{-1} band of MGITC adsorbed on an Au(111) surface. Filled squares and circles represent experimental data, the solid line is a fit curve for a (initial) time constant of 6 s.

In the following we analyze the distinct influence of the spatial intensity distribution on the bleaching rate in more detail in order to extract definite numbers for the spatial extension of the field enhancement in TERS. This will be an extension of the work in Ref. 32, where the field enhancement was modeled by a simple step function.

EM enhancement and bleaching effects of dyes

In general, dyes which are exposed to illumination show bleaching behavior. This effect should not be confused with intensity fluctuations seen in single molecule spectroscopy such as 'blinking'.[14] Of course, in these cases bleaching can also occur in addition. Bleaching means irreversible photo-reaction and photo-degradation of an illuminated dye. In other words, the number of active dye molecules is shrinking during illumination, and this depends on the intensity of illumination at the locations of the molecules, i.e. on the intensity profiles. The analysis of bleaching data can hence provide information about the extent of the enhancement and also on the size of the enhanced electromagnetic field[32] in TERS.

As shown in the Appendix, for a Heaviside profile and a Gaussian profile, the equations for the radius of the enhanced field are the same, in spite of the different nature of the profiles. In contrast, the two profiles lead to different TERS radii (see discussion below). The result for R_{field} for both profiles is

$$R_{field} = \frac{q^{1/2} R_f}{g_{TERS}^2}$$

where q is the net-increase of the Raman scattering induced by the tip, R_f is the radius of the focus and g_{TERS} is the maximum height of the field enhancement profile [see Eqn (A14)]. If we compare the results for the Gaussian and Heaviside profiles, the radius of the enhanced field is the same, whereas the TERS radius R_{TERS} is smaller by a factor of $\frac{1}{2}$ for the former compared with the latter case [simply

because $g \rightarrow g(r)$; see discussion after Eqn (A9)]. This means that the spatial resolution is better by a factor of two than earlier estimated.

Finally, from the fits to Figs 4 and 5 we obtain a field enhancement of the order of $g_{TERS} = 50$, which means a TERS enhancement of ${g_{TERS}}^4 = 6.25 \times 10^6$; the radius of the enhanced field R_{field} is ~50 nm, which results in a TERS radius of 25 nm, which is somewhat smaller than the radius of the tip apex (~30 nm).

CONCLUSIONS

TERS was investigated for MGITC adsorbed at an Au(111) surface with the focus on the bleaching behavior under the influence of enhanced fields. The key conditions for giant TERS are side illumination of the tip, well-prepared single-crystalline surfaces and smooth gold tips with a sharp tip apex. From the bleaching behavior of MGITC, very distinct for the tip-retracted and tip-tunneling conditions, a 50-fold increase of the EM fields at the substrate surface was evaluated. This corresponds to a 2500-fold gain in the light intensity near the tip apex and a TERS enhancement of $\sim 6 \times 10^6$ for dye molecules adsorbed at the Au(111) substrate in a region with 50 nm radius underneath the tip. This enhanced intensity, varying along the surface, causes a fast but locally different bleaching of the dye. It was analyzed in detail for different profiles for the EM field distribution along the substrate surface. Using a Gaussian profile, the time dependencies of the bleaching were modeled, permitting one to reproduce the non-linear slopes of the experimental data in semi-logarithmic plots of both the TERS intensity versus time and the RRS intensity versus time. This provides not only direct insight into the strength of the EM enhancement and the size of the enhanced field but also into some details of the bleaching behavior. The analysis shows, for example, that the bleaching constant is significantly higher for MGITC in an unperturbed environment than for MGITC in an environment which has been substantially bleached. A possible explanation might be that distinct orientations of the dye in these two environments may cause different bleaching rates. The MGITC spectra are also different for these two cases.

Acknowledgements

B.R. gratefully acknowledges the Alexander von Humboldt Foundation for a fellowship and support from the National Science Foundation of China (90206039 and 20473047) and the 973 Project (2001CB610506). G.P. gratefully acknowledges a scholarship from the Max Planck Society.

REFERENCES

1. Stöckle RM, Doug Suh Y, Deckert V, Zenobi R. *Chem. Phys. Lett.* 2000; **318**: 131.
2. Anderson MS. *Appl. Phys. Lett.* 2000; **76**: 3130; *Rev. Sci. Instrum.* 2002; **73**: 1198.
3. Hayazawa N, Inouye Y, Sekhat Z, Kawata S. *Opt. Commun.* 2000; **183**: 333; *Chem. Phys. Lett.* 2001; **335**: 369; *J. Chem. Phys.* 2002; **117**: 1296.
4. Hayazawa N, Tarun A, Inouye Y, Kawata S. *J. Appl. Phys.* 2002; **92**: 6983.
5. Hayazawa N, Yano T, Watanabe H, Inouye Y, Kawata S. *Chem. Phys. Lett.* 2003; **376**: 174.
6. Nieman LT, Krampert GM, Martinez RE. *Rev. Sci. Instrum.* 2001; **72**: 1691.
7. Bulgarevitch DS, Futamata M. *Appl. Spectrosc.* 2004; **58**: 757.
8. Festy F, Demming A, Richards D. *Ultramicrosc.* 2004; **100**: 437.
9. Richards D, Milner RG, Huang F, Festy F. *J. Raman Spectrosc.* 2003; **34**: 663.
10. Pettinger B, Picardi G, Schuster R, Ertl G. *Electrochemistry* 2000; **68**: 942.
11. Pettinger B, Picardi G, Schuster R, Ertl G. *Single Mol.* 2002; **3**: 285.
12. Pettinger B, Picardi G, Schuster R, Ertl G. *J. Electroanal. Chem.* 2003; **554–555**: 293.
13. Jeanmaire DJ, Van Duyne RP. *J. Electroanal. Chem.* 1977; **84**: 1.
14. Nie SM, Emery SR. *Science* 1997; **275**: 1102.
15. Kneipp K, Wang Y, Kneipp H, Perelman LT, Itzkan I, Dasari R, Feld MS. *Phys. Rev. Lett.* 1997; **78**: 1667.
16. Shalaev VM, Sarychev AK. *Phys. Rev. B* 1998; **57**: 13 265.
17. Markel VA, Shalaev VM, Zhang P, Huynh W, Tay L, Haslet TL, Moskovits M. *Phys. Rev. B* 1999; **59**: 10 903.
18. Meixner AJ, Vosgröne T, Sackrow M. *J. Lumin.* 2001; **94–95**: 147.
19. Azoulay J, Debarre A, Richard A, Tchenio P. *J. Microsc.* 1999; **194**: 486.
20. Smith DA, Webster S, Ayat M, Evans SD, Fogherty D, Batchelder B. *Ultramicroscopy* 1995; **61**: 247.
21. Zeisel D, Deckert V, Zenobi R, Vo-Dinh T. *Chem. Phys. Lett.* 1998; **283**: 381.
22. Deckert V, Zeisel D, Zenobi R. *Anal. Chem.* 1998; **70**: 2646.
23. Denk W, Pohl DW. *J. Vac. Sci. Technol. B* 1991; **9**: 645.
24. Zenhausern F, O'Boyle MP, Wickramsinghe HK. *Appl. Phys. Lett.* 1994; **65**: 1623.
25. Jersch J, Demming F, Hildenhagen LJ, Dickmann K. *Appl. Phys. A* 1998; **66**: 29.
26. Demming F, Jersch J, Dickmann K, Geshev PI. *Appl. Phys. B* 1998; **66**: 593.
27. Klein S, Geshev P, Witting T, Dickmann K, Hietschold M. *Electrochemistry* 2002; **71**: 114.
28. Klein S, Witting T, Dickmann K, Geshev P, Hietschold M. *Single Mol.* 2002; **3**: 281.
29. Mills DL. *Phys. Rev. B* 2002; **65**: 125 419.
30. Wu S, Mills DL. *Phys. Rev. B* 2002; **65**: 205 420.
31. Micic M, Klymyshyn N, Suh YD, Lu HP. *J. Phys. Chem. B* 2003; **107**: 1574.
32. Pettinger B, Ren B, Picardi G, Schuster R, Ertl G. *Phys. Rev. Lett.* 2004; **92**: 096 101.
33. Ren B, Picardi G, Pettinger B. *Rev. Sci. Instrum.* 2004; **75**: 837.
34. Ren B, Picardi G, Pettinger B, Schuster R, Ertl G. *Angew. Chem. Int. Ed.* 2004; **44**: 139.
35. Clavilier J, Faure R, Guinet G, Durand R. *J. Electroanal. Chem.* 1980; **107**: 205.

APPENDIX

Reconstructing the original spectra

Already in the first TERS spectra of MGITC recorded within a time series bleaching occurs. Hence the spectroscopic characteristics alter with illumination time, because the local environment of MGITC changes owing to increasing disorder and the newly formed species might also produce

TERS. Assuming that the measured spectra are a linear superposition of the spectra of clean, unbleached MGTIC (I_{MGITC}) and of MGITC in bleached environments (I_{bl}), which presumably does not change significantly during the bleaching process, I_{MGITC} and I_{bl} can be reconstructed from the data by solving a set of two equations.

$$x_1 I_{\mathrm{MGITC}} + x_2 I_{\mathrm{bl}} = I_{\mathrm{TERS},1}$$
$$x_3 I_{\mathrm{MGITC}} + x_4 I_{\mathrm{bl}} = I_{\mathrm{TERS},2}$$

The coefficients x_i ($i = 1, \ldots, 4$) give the fraction of the corresponding species contribution to the spectra $I_{\mathrm{TERS},1}$ and $I_{\mathrm{TERS},2}$. During the initial bleaching processes one can then safely assume that $x_2 = 1 - x_1$ and $x_4 = 1 - x_3$. Hence, on analyzing data from the early bleaching process, only two parameters, x_1 and x_3, have to be estimated, and solving these equations becomes straightforward. For our analysis we used the first two spectra of the time series of Fig. 2. These spectra are similar. Therefore, x_1 and x_3 are fairly large (>0.5), and I_{MGITC} will closely resemble $I_{\mathrm{TERS},1}$ (see Fig. 3 and its discussion).

TIME DEPENDENCE OF BLEACHING PROCESSES

To analyze the observed bleaching behavior, we assume that the bleaching rate of dyes is proportional to the local intensity acting on the dye and the concentration. The proportionality constant is denoted the bleaching constant γ. A differential equation for the time dependence of the dye coverage $\vartheta(t,r,a)$ during illumination describes the decrease of the coverage as being proportional to the product of three terms: for both cases, the tip-retracted case (there is only the resonance Raman scattering by the dye in the laser focus, hence X = RRS and $a = R_{\mathrm{RRS}} = R_{\mathrm{f}}$) and the tip tunneling case (there is the strong enhancement underneath the tip apex, hence, X = TERS and $a = R_{\mathrm{TERS}} = R_{\mathrm{enhanced\ field}}$), we can write

$$\frac{\partial \vartheta_{\mathrm{X}}(t, r, R_{\mathrm{X}})}{\partial t} = \vartheta_{\mathrm{X}}(t, r, R_{\mathrm{X}}) I_{\mathrm{X}}(r, R_{\mathrm{X}}) \gamma \tag{A1}$$

Heaviside profile

First, let us use a Heaviside function for the intensity profile for both cases, i.e. a non-zero constant intensity within the radius R_{X} and zero intensity outside R_{X}. The effect of the bleaching on the coverage of the active dye can then be described by

$$\frac{\partial \vartheta_{\mathrm{X}}}{\partial t} = \vartheta_{\mathrm{X}}(t) I_{\mathrm{X}} \gamma \tag{A2}$$

leading to function decaying exponentially with time:

$$\vartheta_{\mathrm{X}}(t) = \vartheta_0 \, \mathrm{e}^{-I_{\mathrm{X}} \gamma t} \tag{A3}$$

The power radiated by the Raman processes P_{X} for the cases 'tip retracted' and 'tip tunneling' becomes differently time dependent:

$$\begin{aligned} P_{\mathrm{X}} &\approx N_0 \left(\frac{\mathrm{d}\sigma}{\mathrm{d}\Omega}\right) \int_0^{R_{\mathrm{X}}} \vartheta_{\mathrm{X}}(t)\, r\, {g_{\mathrm{X}}}^2\, I_{\mathrm{X}}\, \mathrm{d}r \\ &= N_0 \left(\frac{\mathrm{d}\sigma}{\mathrm{d}\Omega}\right) R_{\mathrm{X}}^2 \pi\, \vartheta_0\, \mathrm{e}^{-I_{\mathrm{X}} \gamma t}\, {g_{\mathrm{X}}}^2\, I_{\mathrm{X}} \end{aligned} \tag{A4}$$

where X denotes either RRS or TERS and N_0 is the surface density of the dye. Note that, the term ${g_{\mathrm{X}}}^2$ in front of I_{X} describes the possible enhancement of the scattered radiation, while the enhancement of the laser light intensity within the region R_{X} is taken into account by I_{X} itself, since $I_{\mathrm{X}} = {g_{\mathrm{X}}}^2 I_{\mathrm{L}}$; hence the enhancements of the bleaching rate and Raman processes are governed by ${g_{\mathrm{X}}}^2$ and ${g_{\mathrm{X}}}^4$, respectively. For the RRS case (tip absent or retracted) $g_{\mathrm{RRS}} = 1$; for the TERS case $g_{\mathrm{TERS}} > 1$. Hence we obtain

$$P_{\mathrm{RRS}} \approx N_0 \left(\frac{\mathrm{d}\sigma}{\mathrm{d}\Omega}\right) {R_{\mathrm{f}}}^2\, \pi\, \vartheta_0\, \mathrm{e}^{-I_{\mathrm{L}} \gamma t}\, I_{\mathrm{L}} \tag{A5}$$

$$P_{\mathrm{TERS}} \approx N_0 \left(\frac{\mathrm{d}\sigma}{\mathrm{d}\Omega}\right) R_{\mathrm{TERS}}^2\, \pi\, {g_{\mathrm{TERS}}}^4\, \vartheta_0\, \mathrm{e}^{-g_{\mathrm{TERS}}^2\, I_{\mathrm{L}} \gamma t}\, I_{\mathrm{L}} \tag{A6}$$

For clarity, we substitute $I_{\mathrm{RRS}} = I_{\mathrm{L}}$ and $R_{\mathrm{RRS}} = R_{\mathrm{f}}$; I_{L} is the average laser intensity in the focal area, which has a radius R_{f}. Analogously, R_{TERS} is the radius of the small area, which contributes to TERS. For a Heaviside field profile the radius of the enhanced field and R_{TERS} have the same value. The ratio for of the radiated Raman powers with an and without tip at $t = 0$ is then given by

$$q = \frac{P_{\mathrm{TERS}}}{P_{\mathrm{RRS}}} = \frac{{R_{\mathrm{TERS}}}^2\, {g_{\mathrm{TERS}}}^2}{{R_{\mathrm{f}}}^2} \tag{A7}$$

If the field enhancement is known from independent measurements, the radius R_{TERS} can be determined:

$$R_{\mathrm{TERS}} = \frac{q^{1/2}\, R_{\mathrm{f}}}{{g_{\mathrm{TERS}}}^2} \tag{A8}$$

Gaussian profile

The derivation of the bleaching-time dependence again becomes simple and straightforward, when using a Gaussian profile. The power radiated by the Raman processes P_{X} can be described as

$$P_{\mathrm{X}} \propto N_0 \left(\frac{\mathrm{d}\sigma}{\mathrm{d}\Omega}\right) 2\pi \int_0^{\infty} \vartheta_{\mathrm{X}}(r, R_{\mathrm{X}}, t)\, {g_{\mathrm{X}}}^2\, I_{\mathrm{X}}\, r\, \mathrm{d}r \tag{A9}$$

where X, N_0, $(\mathrm{d}\sigma/\mathrm{d}\Omega)$, I_{L} and R_{X} have the same meaning as in the former section, while ϑ_{X}, g_{X} and I_{X} become radially varying profiles, where r is the radial coordinate underneath the tip and along the substrate surface. The definitions of the field enhancement and intensity distributions are

$$\begin{aligned} g_{\mathrm{X}}(r) &= \begin{cases} 1 & \mathrm{X} = \mathrm{RRS} \\ 2^{1/2}\, g_0 \exp\left(-\dfrac{r^2}{a^2}\right) & \mathrm{X} = \mathrm{TERS} \end{cases} \\ I_{\mathrm{X}}(r) &= \begin{cases} 2 I_{\mathrm{L}} \exp\left(-\dfrac{r^2}{{R_{\mathrm{f}}}^2}\right) & \mathrm{X} = \mathrm{RRS} \\ 2 I_{\mathrm{L}}\, 2\, {g_0}^2 \exp\left(-\dfrac{2r^2}{a^2}\right) & \mathrm{X} = \mathrm{TERS} \end{cases} \end{aligned} \tag{A10}$$

where $g_0 = g_{TERS}$, to simplify the notation. Note the factors $2^{1/2}$ and 2 in Eqn (A10). They ensure that the Gaussian field profile produces the same avarage intensity as the Heaviside profile having the amplitude g_0 or I_L. Note also that in the TERS case the tip is placed in the focus center; hence the incident intensity near the tip is $2I_L$. Because of the illumination and the varying field strength along r, the number of unbleached molecules in each element $r\mathrm{d}r$ depends on the local intensity of the incident light and the exposure time t via an exponential term $N \rightarrow N_X(r,t) = N_0\,\vartheta_X\,(r, R_X, t) = N_0 \exp[-\exp(-2r^2/{R_f}^2)2I_L\gamma\,t]$, where γ is the bleaching constant and the factor 2 in front of r^2 arises because the local intensity is proportional to field squared. Hence

$$P_{RRS}(R_f,t) \propto N_0\left(\frac{\mathrm{d}\sigma}{\mathrm{d}\Omega}\right) 2{I_L}^* \; 2\pi\int_0^\infty \mathrm{e}^{-\mathrm{e}^{-2r^2/{R_f}^2}\,2I_L\gamma t-2r^2/{R_f}^2}\, r\,\mathrm{d}r = N_0\left(\frac{\mathrm{d}\sigma}{\mathrm{d}\Omega}\right){R_f}^2\,\pi\,I_L\frac{1-\mathrm{e}^{-2I_L\gamma t}}{2I_L\gamma t} \qquad \text{(A11a)}$$

From this analytical expression, one obtains in the limit of $t \rightarrow 0$

$$P_{RRS}(R_f,0) = N_0\left(\frac{\mathrm{d}\sigma}{\mathrm{d}\Omega}\right){R_f}^2\pi\,I_L \qquad \text{(A11b)}$$

Similarly for the TERS case one can find the analytical expression for the integral in Eqn (A9). This leads in the limit of $t \rightarrow 0$ to

$$P_{TERS}(a,0) \propto N_0\left(\frac{\mathrm{d}\sigma}{\mathrm{d}\Omega}\right)4g_0^4\,2I_L \times \lim_{t\longrightarrow 0}(2\pi\int_0^\infty \mathrm{e}^{-\mathrm{e}^{-2r^2/a^2}\,2\,{g_0}^2\,2I_L\gamma t-4r^2/a^2}\,r\mathrm{d}r) = N_0\left(\frac{\mathrm{d}\sigma}{\mathrm{d}\Omega}\right)g_0^4\,2I_L\,a^2\pi \qquad \text{(A12)}$$

where $a = R_{field}$ is the radius of the enhanced field and $g_0 = g_{TERS}$ is the enhancement factor at the profile maximum. Next, one has take into account, that the local incident intensity near the tip is $\sim 2I_L$, whereas for the RRS case the avarage intensity is I_L. Hence the ratio q is

$$q = \frac{P_{TERS}(a,0)}{2P_{RRS}(R_f,0)} = \frac{{g_0}^4\,a^2}{{R_f}^2} \qquad \text{(A13)}$$

where the factor 2 in the denominator corrects for the different operating intensities. For the enhanced field radius a we find

$$a = R_{field} = \frac{q^{1/2}\,R_f}{{g_{TERS}}^2} \qquad \text{(A14)}$$

which is the same as found for a Heaviside profile. However, the use of r-dependent profiles leads to a smaller radius for TERS, because of the definition of $g(r) = 2^{1/2}g_0\exp(-r^2/{R_{field}}^2)$, yielding $g^4(r) = 4\,{g_0}^4\exp(-4r^2/{R_{field}}^2) = 4\,{g_0}^4\exp(-r^2/{R_{TERS}}^2)$. Hence $R_{TERS} = \frac{1}{2}R_{field}$. Therefore, if $R_{field} \approx 50$ nm, then $R_{TERS} \approx 25$ nm. The important consequence is that TERS exhibits a higher spatial resolution than estimated from a Heaviside profile.

Comparison of Gaussian and simple EM model profiles

The Gaussian profiles used here are approximations for the field distributions, which are certainly better ones than simple step functions. However, the question has to be answered of whether they are adequate. For this purpose, let us substitute the tip by a small sphere over the substrate with its radius much smaller than the excitation wavelength: $R_s \ll \lambda$. Since we are interested in the distance dependence of the enhancement, we can resort to a simple model for the EM enhancement along that used by Kerker and Blatchford.[A1] They describe the enhancement as a near-field interaction of an oscillating dipole located in the center of the sphere with a molecule outside the sphere. The distance dependence is basically given by

$$g_{inc} = g_0\left(\frac{R_s}{R}\right)^3; g_{sc} = g_0\left(\frac{R_s}{R}\right)^3$$

Hence, the distance dependence of TERS exhibits an R^{-12} dependence, which is certainly valid only for small tip radii. In our case, the sphere is located at a distance d ($\sim$1 nm) above the substrate and the molecules are located on the substrate surface, thus $R = [(R_s + d)^2 + r]^{1/2}$, where r is the radial distance along the surface. Underneath the sphere (the tip) and along the substrate surface a large number of molecules are located, which experience locally different field enhancements. Since we are only interested in the TERS profile, we present the enhancement–r dependence as a normalized quantity:

$$F_{TERS}(r) = \frac{5{r_0}^{10}}{{R_s}^{12}\,{g_0}^4\pi}\int_r^\infty\left(\frac{{g_0}^{3/2}}{{r_0}^2+x^2}\right)^6 2\pi\,x\,\mathrm{d}x = (1 + r^2/{r_0}^2)^{-5} \qquad \text{(A15)}$$

where we use $r_0 = R_s + d$. Here, $F_{TERS}(r)$ indicates the fraction of the enhancement present in the ring area with an inner radius r and an outer radius of infinity. This normalization has the advantage that the normalized profile becomes independent of some unknown quantities not accessible in the framework of this model, such as R_s, the height of the field enhancement and the resonance frequency. Figure A1 shows two profiles for $R_s = 30$ and 50 nm, $d = 1$ nm, together with two Gaussian profiles with $a = 15$ and 25 nm, respectively. Evidently, each set of profiles nearly matches, indicating a TERS radius of about 15 or 25 nm, which is about half the sphere radius. One should note that the used model does not take into account either the influence of the metal surface on the field distribution or the orientation of the

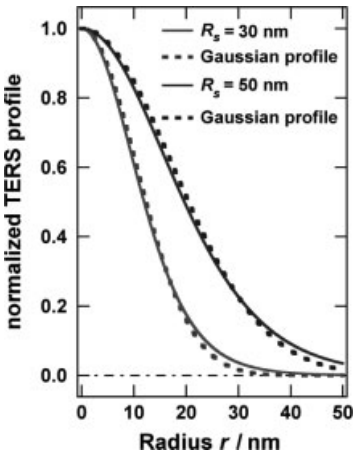

Figure A1. Normalized TERS enhancement profiles vs the radial distance r along the substrate surface. The profiles (solid lines) are calculated according to Eqn (A15) for $R_s = 30$ and 50 nm. For comparison, Gaussian profiles are given with $a = 15$ and 25 nm.

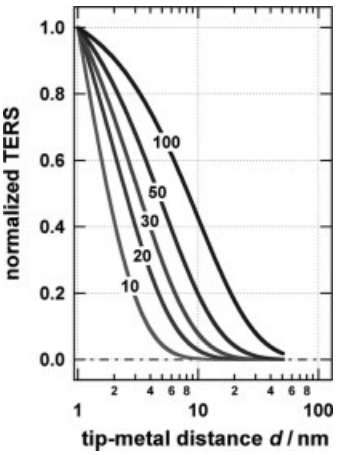

Figure A2. Normalized TERS intensity vs tip–substrate distance d for different sphere radii according to Eqn (A16).

field. Presumably, these effects sharpen the field profiles. On the other hand, considering the real shape of the tip may make these profiles less sharp. Therefore, we can consider Eqn (A15) as a fairly good approximation for $F_{TERS}(r)$. The same holds then for an appropriate Gaussian profile.

Another important question concerns the dependence of the enhancement on the tip – metal separation s (for $s \geq d$). To answer this at least partly, we normalize the enhancement in a different way, taking as reference the enhancement at the closest distance which is about $d \approx 1$ nm:

$$\frac{F_{TERS}(s \geq d)}{F_{TERS}(d)} = \frac{\int_0^\infty \left(\frac{{g_1}^{3/2} {R_s}^2}{{r_1}^2 + x^2} \right)^6 2\pi\, x\, dx}{\int_0^\infty \left(\frac{{g_0}^{3/2} {R_s}^2}{{r_0}^2 + x^2} \right)^6 2\pi\, x\, dx} = (R_s + d)^{10}\,(R_s + s)^{-10} \quad \text{(A16)}$$

with $g_1 = g_0$ and $r_1 = R_s + s$. This distance dependence exhibits a fast decay of the normalized TERS signal within a few nanometers, as shown in Fig. A2 for different sphere radii. The results of this simple model are in fairly good agreement with the distance dependence reported by Hartschuh *et al*.[A2] shown in Fig. A3, for TERS of a single SWNT (single-wall nanotube) on a glass substrate monitored by a silver tip with 10–15 nm radius. Not included in our model is the change of the LSP resonance with increasing distance, which should move towards the visible region and could compensate the decay of the TERS signal to some extent. From the close relationship between the experimental and modeled curves, we conclude that the dependence of TERS on the tip–sample distance is mainly controlled by the distance dependence of the near-field processes.

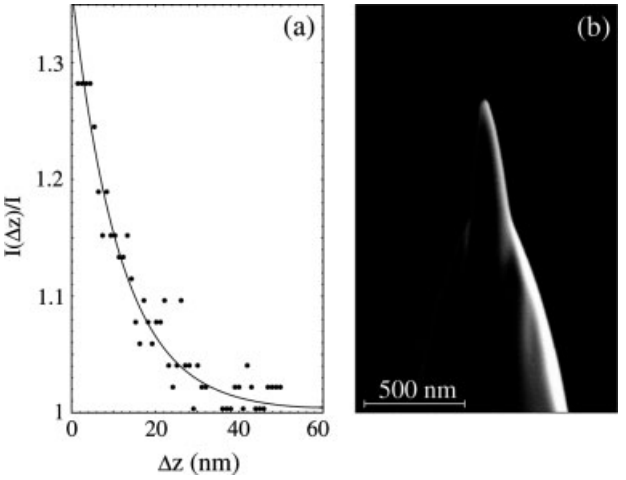

Figure A3. (a) Dependence of the Raman scattering strength of the G band (I) on the longitudinal separation $\Delta(z)$ between a single SWNT and the tip. The solid line is an exponential fit with a decay length of 11 nm. The signal is normalized with the far-field signal. (b) Scanning electron micrograph of a sharp silver tip fabricated by focused ion beam milling. (Reprinted with permission from Ref. A2).

REFERENCES

A1. Kerker M, Blatchford CG. *Phys. Rev. B* 1982; **26**: 4052.
A2. Hartschuh A, Sánchez EJ, Xie XS, Novotny L. *Phys. Rev. Lett.* 2003; **90**: 095 503.